AN ACCURATE SOLUTION TO THE MESHLESS LOCAL PETROV-GALERKIN FORMULATION IN ELASTODYNAMICS

Chyou-Chi Chien* and Tong-Yue Wu

ABSTRACT

A meshless local Petrov-Galerkin (MLPG) method for solving elastodynamic problems is developed and numerically implemented. The proposed MLPG approach is based on a locally symmetric weak form and shape functions from the moving least squares (MLS) approximation. This approach is truly meshless, as it does not involve a finite element mesh, either to interpolate the solution variables, or to integrate the energy. However, complex vibrating-modes or -frequencies may arise from asymmetric mass and stiffness matrices formulated by the MLPG method. Unlike the commonly used finite difference methods such as the Newmark method, the accurate approach in this study is the time-discontinuous Galerkin (TDG) method for solving second-order ordinary differential equations in the time domain. Numerical results indicate that the TDG method provides very stable and accurate results in the sense that the crucial modes are accurately integrated and the spurious modes are successfully filtered out.

Key Words: meshless local Petrov-Galerkin (MLPG) method, time-discontinuous Galerkin (TDG) method, elastodynamics.

I. INTRODUCTION

Meshless methods have become very attractive and efficient for developing adaptive methods for solving boundary value problems because nodes can easily be added and removed without burdensome remeshing of the elements. The meshless local Petrov-Galerkin approach (Atluri and Zhu, 1998; 2000), based on the local symmetric weak form (LSWF) and the moving least squares (MLS) approximation, is a truly numerical meshless method for solving boundary value problems. The primary advantage of this method over the extensively used finite element method and other so-called meshless methods such as the diffuse element method (Nayroles *et al*., 1992), the element free Galerkin method (Belytschko *et al*., 1994; Zhu and Atluri, 1998), and the reproducing kernel particle method (Liu *et al*., 1995), is that it does not require a finite element mesh, either to interpolate the solution variables, or to integrate the energy. Recently, a meshless local boundary integral equation method with the Houbolt finite difference scheme was successfully applied to solve 2D elastodynamic problems (Sladek *et al*., 2003).

In this present study, the MLPG approach for solving problems in elastodynamics is developed. The method utilizes a local symmetric weak form (LSWF) and shape functions from the MLS approximation. In the present formulation, the test and trial functions are selected from different functional spaces, and the trial functions are approximated by the MLS approximation, while the test functions are some kinds of known functions. A penalty formulation is used to enforce the essential boundary conditions in the present method, since the essential boundary conditions cannot be directly imposed when the MLS approximation is used to approximate the displacement variables. As was stated in Atluri and Zhu (1998), this MLPG method for solving problems in elastodynamics is a truly meshless method, and needs absolutely no meshes of either the traditional finite-element or the boundary-element type, either to interpolate the solution variables, or to integrate the energy. The formulation involves only domain and

*Corresponding author. (Tel: 886-3-2654200; Email: chyouchi@cycu.edu.tw)

C. C. Chien is with the Department of Civil Engineering, Chung-Yuan University, Chung-Li, Taiwan 320, R.O.C.

T. Y. Wu is with the Department of Mechanical Engineering, Chung-Yuan University, Chung-Li, Taiwan 320, R.O.C.

boundary integrals over very regular sub-domains and their boundaries. These integrals can be easily and directly evaluated over the very regular shapes of the sub-domains and their boundaries.

This work adopts a time-discontinuous Galerkin method unlike commonly used finite difference methods, such as the Newmark method, to solve second-order ordinary differential equations in the time domain. This formulation is solved by the time-discontinuous Galerkin method in which both the unknown displacements and unknown velocities are approximated as piecewise linear interpolation functions in the time domain. Numerical results demonstrate that the TDG method yields very stable and accurate results in the sense that the crucial modes have been accurately integrated and the spurious ones successfully filtered out.

II. MOVING LEAST SQUARE (MLS) APPROXIMATION

Consider a sub-domain Ω_k, the neighborhood of a point $\boldsymbol{k}$, and the domain of the definition of the MLS approximation for the trial function at $\boldsymbol{x}$, which is located in the problem domain $\boldsymbol{\Omega}$ (Lancaster and Salkauskas, 1981). To approximate the distribution of function u in Ω_k, the moving least squares approximant $f^h(\boldsymbol{x})$ of u, can be defined as follows, over a number of randomly located nodes $\{\boldsymbol{x}_i\}$, i=1, 2, ⋯, n;

$$f^h(\boldsymbol{x})=\boldsymbol{p}^T(\boldsymbol{x})\boldsymbol{a}(\boldsymbol{x}),\ \forall x\in \Omega_k \tag{1}$$

where $\boldsymbol{p}^T(\boldsymbol{x})=[p_1(\boldsymbol{x}), p_2(\boldsymbol{x}), \cdots, p_m(\boldsymbol{x})]$ is a complete monomial basis of order m; and $\boldsymbol{a}(\boldsymbol{x})$ is a vector of coefficients $a_j(\boldsymbol{x})$, j=1, 2, ⋯, m, which are functions of the space coordinates $\boldsymbol{x}=[x, y, z]^T$. For 2-D problems,

linear basis: $\boldsymbol{p}^T(\boldsymbol{x})=[1, x, y]$, m=3 (2a)

quadratic basis: $\boldsymbol{p}^T(\boldsymbol{x})=[1, x, y, xy, x^2, y^2]$, m=6 (2b)

The coefficient vector $\boldsymbol{a}(\boldsymbol{x})$ is determined by minimizing a weighted discrete L_2 norm, defined as,

$$I(\boldsymbol{x}) = \sum_{i=1}^{n} w_i(\boldsymbol{x})[\boldsymbol{p}^T(\boldsymbol{x}_i)\boldsymbol{a}(\boldsymbol{x}) - \hat{f}_i]^2$$

$$= [\boldsymbol{P}\cdot\boldsymbol{a}(\boldsymbol{x}) - \hat{\boldsymbol{f}}]^T\cdot\boldsymbol{W}\cdot[\boldsymbol{P}\cdot\boldsymbol{a}(x) - \hat{\boldsymbol{f}}] \tag{3}$$

where $w_i(\boldsymbol{x})$ is the weight function associated with the node i, with $w_i(\boldsymbol{x})>0$ for all $\boldsymbol{x}$ in the (compact) support of $w_i(\boldsymbol{x})$, where w_i represents the value of $\boldsymbol{x}$ at node i, and n is the number of nodes in Ω_k for which the weight functions $w_i(\boldsymbol{x})>0$.

Here, the matrices $\boldsymbol{P}$ and $\boldsymbol{W}$ can be expressed as,

$$\boldsymbol{P} = \begin{bmatrix} \boldsymbol{p}^T(\boldsymbol{x}_1) \\ \boldsymbol{p}^T(\boldsymbol{x}_2) \\ \cdots \\ \boldsymbol{p}^T(\boldsymbol{x}_n) \end{bmatrix}_{n\times m} \tag{4}$$

and

$$\boldsymbol{W} = \begin{bmatrix} w_1(\boldsymbol{x}) & \cdots & 0 \\ \vdots & \ddots & \vdots \\ 0 & \cdots & w_n(\boldsymbol{x}) \end{bmatrix} \tag{5}$$

Notably, $\hat{f}_i$, i=1, 2, ⋯, n in Eq. (3) are fictitious nodal values, and are not the nodal values of the unknown trial function $f^h(\boldsymbol{x})$ in general;

$$\hat{\boldsymbol{f}}^T = \left\lfloor \hat{f}_1, \hat{f}_2, \cdots, \hat{f}_n \right\rfloor \tag{6}$$

Using $I(\boldsymbol{x})$ in Eq. (3), take stationarity for $\boldsymbol{a}(\boldsymbol{x})$ in the form of,

$$\frac{\partial I(\boldsymbol{x})}{\partial \boldsymbol{a}(\boldsymbol{x})} = 0 \tag{7}$$

Therefore,

$$\boldsymbol{A}(\boldsymbol{x})\boldsymbol{a}(\boldsymbol{x}) = \boldsymbol{B}(\boldsymbol{x})\hat{\boldsymbol{f}} \tag{8a}$$

or

$$\boldsymbol{a}(\boldsymbol{x}) = \boldsymbol{A}^{-1}(\boldsymbol{x})\boldsymbol{B}(\boldsymbol{x})\hat{\boldsymbol{f}} \tag{8b}$$

$$\boldsymbol{A}(\boldsymbol{x})=\boldsymbol{P}^T\boldsymbol{W}\boldsymbol{P}=\boldsymbol{B}\boldsymbol{P} \tag{9}$$

$$\boldsymbol{B}(\boldsymbol{x})=\boldsymbol{P}^T\boldsymbol{W} \tag{10}$$

Substituting Eq. (8b) into Eq. (1), it yields,

$$f^h(\boldsymbol{x}) = \boldsymbol{\Phi}^T(\boldsymbol{x})\hat{\boldsymbol{f}} = \sum_{j=1}^{N} \phi_j\hat{f}_j\,,\quad \forall \boldsymbol{x}\in\Omega_k \tag{11}$$

where

$$\boldsymbol{\Phi}^T(\boldsymbol{x})=\boldsymbol{P}^T(\boldsymbol{x})\boldsymbol{A}^{-1}(\boldsymbol{x})\boldsymbol{B}(\boldsymbol{x}) \tag{12}$$

is called the nodal shape function. Its derivatives can be written as,

$$\frac{\partial\boldsymbol{\Phi}}{\partial x_i} = \boldsymbol{\Phi}_{,i} = \boldsymbol{P}^T_{,i}\boldsymbol{A}^{-1}\boldsymbol{B} + \boldsymbol{P}^T(\boldsymbol{A}^{-1}\boldsymbol{B}_{,i} + \boldsymbol{A}^{-1}{}_{,i}\boldsymbol{B}) \tag{13}$$

in which stationarity

$$\boldsymbol{A}^{-1}{}_{,i}=-\boldsymbol{A}^{-1}\boldsymbol{A}_{,i}\boldsymbol{A}^{-1} \tag{14}$$

The MLS approximation is well defined only when the matrix $\boldsymbol{A}$ in Eq. (14) is non-singular (Nayroles *et al*., 1992). A necessary condition for a well-defined MLS approximation is that at least m weight functions are non-zero ($n>m$) for each sample point $\boldsymbol{x}$ in Ω, and that the nodes in Ω_k, are not arranged in a special pattern, such as on a straight line (Belytschko *et al*., 1996; Breitkopf *et al*., 2000).

In implementing the MLS approximation, the basis functions and weight functions should be chosen first. The spline weight function with compact supports is considered in the present work. The spline weight function, corresponding to node i can be written as (Atluri *et al*., 1999)

$$w_i(\boldsymbol{x})=\begin{cases} 1-6(\frac{d_i}{r_i})^2+8(\frac{d_i}{r_i})^3-3(\frac{d_i}{r_i})^4 & 0\le d_i\le r_i \\ 0 & d_i\ge r_i \end{cases} \tag{15}$$

where $d_i=|\boldsymbol{x}-\boldsymbol{x_i}|$ is the distance from node x_i to point $\boldsymbol{x}$.

III. MESHLESS LOCAL PETROV-GALERKIN FORMULATION FOR ELASTODYNAMICS

Consider a 2-D linear elastodynamic problem in the domain Ω:

$$\sigma_{ij,\,j}+b_i=\rho\ddot{u}_i \tag{16}$$

where σ_{ij} is the stress tensor, which corresponds to the displacement field u_i; b_i is the body force, $\ddot{u}_i$ is the acceleration field; and $(\,)i$ denotes $(\,)/x_i$. The corresponding boundary conditions are given as follows:

$$u_i=\overline{u}_i \text{ on } \Gamma_u \tag{17a}$$

$$t_i\equiv\sigma_{ji}n_j=\overline{t}_i \text{ on } \Gamma_t \tag{17b}$$

where $\overline{u}_i$ and $\overline{t}_i$ are the prescribed displacements and tractions, respectively, on the displacement boundary Γ_u and on the traction boundary Γ_t, and n_j is the unit outward normal to the boundary Γ.

The domain Ω is subjected to the following initial conditions:

$$u_i(x,\,0)=\boldsymbol{u}_0 \tag{18a}$$

$$\dot{u}_i(x,\,0)=\boldsymbol{v}_0 \tag{18b}$$

where $\boldsymbol{u}_0$ and $\boldsymbol{v}_0$ are the prescribed initial displacement and initial velocity, respectively.

In the Galerkin finite element and element free Galerkin methods, which are both based on the global Galerkin formulation, the global weak form over the entire domain Ω is used to solve the problem numerically. In the present local Petrov-Galerkin formulation, a weak form over a local subdomain Ωs, is first determined, and the MLS approximation is used to develop a truly meshless method, where the local sub-domain Ωs, is located entirely within the global domain Ω. The local sub-domain Ωs is conveniently assumed to be a sphere in 3-D, or a circle in 2-D centered at the point $\boldsymbol{x}$ in question. A generalized local weak form of the differential equation and the boundary conditions, over a local sub-domain Ωs, can be written as,

$$\int_{\Omega_s}(\sigma_{ij,\,j}+b_i-\rho\ddot{u}_i)\delta u_i d\Omega-\kappa\int_{\gamma_u}(u_i-\overline{u}_i)\delta u_i d\gamma=0 \tag{19}$$

where u_i and δu_i are the trial and test functions, respectively, κ is a penalty parameter and γ_u is a part of the boundary of Ωs, over which the essential boundary conditions are specified.

Using the integration by parts in Eq. (19) yields,

$$\int_{\gamma}(\sigma_{ij}n_j)\delta u_i d\gamma-\int_{\Omega_s}(\sigma_{ij}\delta u_{i,\,j}-b_i\delta u_i+\rho\ddot{u}_i\delta u_i)d\Omega$$

$$-\kappa\int_{\gamma_u}(u_i-\overline{u}_i)\delta u_i d\gamma=0 \tag{20}$$

It should be noted that Eq. (20) applies, independent of the size and shape of Ωs. Then, imposing the natural boundary conditions, one obtains,

$$\int_{\gamma_d}t_i\delta u_i d\gamma+\int_{\gamma_t}\overline{t}_i\delta u_i d\gamma+\int_{\gamma_u}t_i\delta u_i d\gamma$$

$$-\int_{\Omega_s}(\sigma_{ij}\delta u_{i,\,j}-b_i\delta u_i+\rho\ddot{u}_i\delta u_i)d\Omega$$

$$-\kappa\int_{\gamma_u}(u_i-\overline{u}_i)\delta u_i d\gamma=0 \tag{21}$$

where $\gamma_d\subset\gamma$ and $\gamma=\gamma_d+\gamma_u+\gamma_t$. Notably, the boundaries $\gamma_u=\gamma\cap\Gamma_u$ and $\gamma_t=\gamma\cap\Gamma_t$, as depicted in Fig. 1.

The test functions δu_i are deliberately selected such that they vanish over r_d, the circle (for an internal node) or the circular arc (for a node on the global boundary), to simplify the above equation. This simplification can be easily accomplished using the weight function in the MLS approximation also as a test function, with the radius r_i of the support of the weight function being replaced by the radius r_o of the local domain Ωs, such that the test function vanishes on r_d. Using these test functions and rearranging Eq.

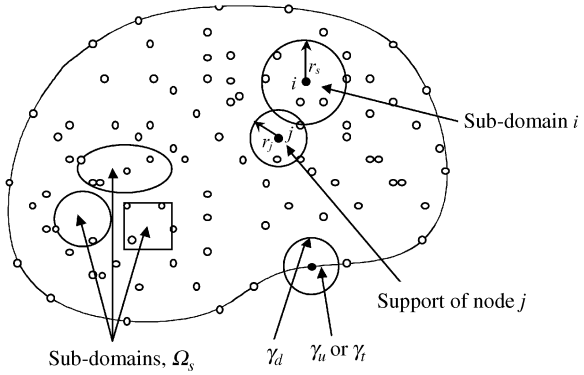

Fig. 1 Sub-domain Ω_s, boundary of sub-domain (including γ_d, γ_u, and γ_t), and support region of node j

(21) yields, the following local symmetric weak form (LSWF) in linear elastodynamics,

$$\int_{\Omega_s}(\sigma_{ij}\delta u_{i,j}+\rho\ddot{u}_i\delta u_i)d\Omega+\kappa\int_{\gamma_u}u_i\delta u_i d\gamma-\int_{\gamma_u}t_i\delta u_i d\gamma$$

$$=\int_{\gamma_t}\overline{t}_i\delta u_i d\gamma+\kappa\int_{\gamma_u}\overline{u}_i\delta u_i d\gamma+\int_{\Omega_s}b_i\delta u_i d\Omega \quad (22)$$

Two (for 2-D problems) or three (for 3-D problems) independent sets of test functions in Eq. (22) can be applied to give,

$$\int_{\Omega_s}(\sigma_{ij}\delta u_{li,j}+\rho\ddot{u}_i\delta u_{li})d\Omega+\kappa\int_{\gamma_u}u_i\delta u_{li}d\gamma$$

$$-\int_{\gamma_u}t_i\delta u_{li}d\gamma$$

$$=\int_{\gamma_t}\overline{t}_i\delta u_{li}d\gamma+\kappa\int_{\gamma_u}\overline{u}_i\delta u_{li}d\gamma+\int_{\Omega_s}b_i\delta u_{li}d\Omega \quad (23)$$

where δu_{li} denotes the ith component of the test function in the lth set. For brevity, Eq. (23) can also be written in matrix form as,

$$\int_{\Omega_s}\delta\boldsymbol{\varepsilon}^T:\boldsymbol{\sigma}d\Omega+\int_{\Omega_s}\rho\delta\boldsymbol{u}^T:\ddot{\boldsymbol{u}}d\Omega+\kappa\int_{\gamma_u}\delta\boldsymbol{u}^T\cdot\boldsymbol{u}d\gamma$$

$$-\int_{\gamma_u}\delta\boldsymbol{u}^T\cdot\boldsymbol{t}d\gamma$$

$$=\int_{\gamma_t}\delta\boldsymbol{u}^T\cdot\overline{\boldsymbol{t}}\,d\gamma+\kappa\int_{\gamma_u}\delta\boldsymbol{u}^T\cdot\overline{\boldsymbol{u}}\,d\gamma+\int_{\Omega_s}\delta\boldsymbol{u}^T\cdot\boldsymbol{b}\delta d\Omega \quad (24)$$

where $\delta\varepsilon^T$ represents the strain matrix from the test functions, and σ denotes the stress vector from the trial functions.

For each i sub-region, substituting f^h for u^h and $\ddot{u}^h$ in Eq. (11) into Eq. (24) and integrating, yields,

$$\sum_{j=1}^{N}m_{ij}\ddot{\hat{u}}_j+\sum_{j=1}^{N}k_{ij}\hat{u}_j=f_i,\quad i=1,2,\cdots,N \quad (25)$$

where N is the number of nodes. The matrix form of Eq. (25) can be expressed in,

$$\boldsymbol{M}\ddot{\hat{\boldsymbol{u}}}+\boldsymbol{K}\hat{\boldsymbol{u}}=\boldsymbol{F} \quad (26)$$

where $\boldsymbol{m}_{ij}$ is defined as,

$$\boldsymbol{m}_{ij}=\rho\int_{\Omega_s}\boldsymbol{\Psi}_i^T\boldsymbol{\Phi}_j d\Omega \quad (27)$$

and,

$$\boldsymbol{\Psi}_i=\begin{bmatrix}w_i & 0\\ 0 & w_i\end{bmatrix};\quad \boldsymbol{\Phi}_j=\begin{bmatrix}\phi_j & 0\\ 0 & \phi_j\end{bmatrix} \quad (28)$$

The matrix in Eq. (25), $\boldsymbol{k}_{ij}$ is defined as,

$$\boldsymbol{k}_{ij}=\int_{\Omega_s}\overline{\boldsymbol{B}}_i^T\boldsymbol{D}\boldsymbol{B}_j d\Omega+\kappa\int_{\gamma_u}\boldsymbol{\Psi}_i^T\boldsymbol{\Phi}_j d\gamma$$

$$-\int_{\gamma_u}\boldsymbol{\Psi}_i^T\boldsymbol{N}\boldsymbol{D}\boldsymbol{B}_j d\gamma \quad (29)$$

if node i is on the boundary

$$\boldsymbol{k}_{ij}=\int_{\Omega_s}\overline{\boldsymbol{B}}_i^T\boldsymbol{D}\boldsymbol{B}_j d\Omega \quad (30)$$

if node i is in the interior

in which,

$$\overline{\boldsymbol{B}}_i=\begin{bmatrix}w_{i,1} & 0\\ 0 & w_{i,2}\\ w_{i,2} & w_{i,1}\end{bmatrix};\ \boldsymbol{B}_j=\begin{bmatrix}\phi_{j,1} & 0\\ 0 & \phi_{j,2}\\ \phi_{j,2} & \phi_{j,1}\end{bmatrix};$$

$$\boldsymbol{N}=\begin{bmatrix}n_1 & 0 & n_2\\ 0 & n_2 & n_1\end{bmatrix} \quad (31)$$

$$\boldsymbol{D}=\frac{\tilde{E}}{1-\tilde{\nu}^2}\begin{bmatrix}1 & \tilde{\nu} & 0\\ \tilde{\nu} & 1 & 0\\ 0 & 0 & (1-\tilde{\nu})/2\end{bmatrix} \quad (32)$$

and

$\tilde{E}=E,\ \tilde{\nu}=\nu$ for the state of plane stress

$\tilde{E}=\dfrac{E}{1-\nu^2},\ \tilde{\nu}=\dfrac{\nu}{1-\nu}$ for the state of plane strain (33)

The load vector is defined as follows:

$$\boldsymbol{f}_i = \int_{\gamma_t} \boldsymbol{\Psi}_i^T \overline{\boldsymbol{t}}\, d\gamma + \kappa \int_{\gamma_u} \boldsymbol{\Psi}_i^T \overline{\boldsymbol{u}}\, d\gamma + \int_{\Omega_s} \boldsymbol{\Psi}_i^T \boldsymbol{b} d\Omega \tag{34}$$

if node i is on the boundary

$$\boldsymbol{f}_i = \int_{\Omega_s} \boldsymbol{\Psi}_i^T \boldsymbol{b} d\Omega \tag{35}$$

if node i is in the interior

where

$$\boldsymbol{b} = \begin{bmatrix} b_1 \\ b_2 \end{bmatrix} \tag{36}$$

Clearly, the system stiffness matrix used in the present method is banded but asymmetric. The locations of the non-zero entries in the system "stiffness" matrix depend on the nodes located inside the domain of influence of the node. However, under some limitations, the system stiffness matrix used in the present method can behave as symmetric and banded (Atluri *et al.*, 1999).

Notably, the prescribed initial displacement and velocity vectors must be converted into the following forms and can match Eq. (26) to solution, such as,

$$\hat{\boldsymbol{u}}_0 = \boldsymbol{T}\boldsymbol{u}_0 \tag{37a}$$

$$\hat{\boldsymbol{v}}_0 = \boldsymbol{T}\boldsymbol{v}_0 \tag{37b}$$

in which,

$$\boldsymbol{T}_{N\times N} = \begin{bmatrix} \boldsymbol{\Phi}_{1j} \\ \boldsymbol{\Phi}_{2j} \\ \vdots \\ \boldsymbol{\Phi}_{Nj} \end{bmatrix}^{-1}, \quad j=1, 2, \cdots, N \tag{38}$$

The relative errors and convergence efficiency of the MLPG method are explained in the reference of Atluri and Zhu, 2000.

IV. TIME-DISCONTINUOUS GALERKIN FINITE ELEMENT METHOD

Let $0=t_1<t_2<\cdots<t_n<t_{n+1}<\cdots<t_{N+1}=T$ be a partition of the time domain $I=(0, T)$ with corresponding time steps $\Delta t_n=t_{n+1}-t_n$ and $I_n=(t_n, t_{n+1})$. Let the time finite element space be described by:

$$\boldsymbol{V}^h = \{\boldsymbol{w}^h = \bigcup_{n=1}^{N} (P^k(I_n))^{n_{eq}}\} \tag{39}$$

where P^k represents the kth-order polynomial, and each member of $\boldsymbol{V}^h$ is a vector that consists of n_{eq} linear functions on each time step I_n. All trial displacements and velocities and their corresponding weighting functions are chosen from the space $\boldsymbol{V}^h$. Notably, the functions in $\boldsymbol{V}^h$ may be discontinuous at the discrete time levels t_n. Therefore, the following notation is introduced,

$$\boldsymbol{w}_n^+ = \lim_{\varepsilon \to 0^+} \boldsymbol{w}(t_n + \varepsilon) \tag{40a}$$

$$\boldsymbol{w}_n^- = \lim_{\varepsilon \to 0^-} \boldsymbol{w}(t_n + \varepsilon) \tag{40b}$$

$$[\boldsymbol{w}_n] = \boldsymbol{w}_n^+ - \boldsymbol{w}_n^- \tag{40c}$$

where $[\boldsymbol{w}_n]$ represents the jump of $\boldsymbol{w}_n$ at t_n, and the inner product on I_n is denoted by:

$$(\boldsymbol{w}, \boldsymbol{u})_{I_n} = \int_{I_n} \boldsymbol{w} \cdot \boldsymbol{u}\, dt \tag{41}$$

The time-discontinuous Galerkin finite element method can now be formulated to solve Eq. (26) as follows.

Find $\boldsymbol{U}^h=\{\boldsymbol{u}^h, \boldsymbol{v}^h\} \in \boldsymbol{V}^h \times \boldsymbol{V}^h$ such that for all $\boldsymbol{W}^h=\{\boldsymbol{w}_1^h, \boldsymbol{w}_2^h\} \in \boldsymbol{V}^h \times \boldsymbol{V}^h$,

$$\begin{aligned} R_n = &\int_{I_n} \boldsymbol{w}_2^h \cdot (\boldsymbol{L}_1\boldsymbol{U}^h - \boldsymbol{F}) dt + \int_{I_n} \boldsymbol{w}_1^h \cdot \boldsymbol{K}\boldsymbol{L}_2\boldsymbol{U}^h dt + \boldsymbol{w}_1^h(t_n^+) \\ &\cdot \boldsymbol{K}[\hat{\boldsymbol{u}}^h(t_n^+) - \hat{\boldsymbol{u}}^h(t_n^-)] + \boldsymbol{w}_2^h(t_n^+) \\ &\cdot \boldsymbol{M}[\hat{\boldsymbol{v}}^h(t_n^+) - \hat{\boldsymbol{v}}^h(t_n^-)] = 0 \quad n=1, 2, \ldots, N \end{aligned} \tag{42}$$

where $\boldsymbol{w}_1^h$ and $\boldsymbol{w}_2^h$ are the weight functions that correspond to the displacement and velocity, respectively, and

$$\boldsymbol{L}_1\boldsymbol{U}^h = \boldsymbol{M}\dot{\hat{\boldsymbol{v}}}^h + \boldsymbol{K}\hat{\boldsymbol{u}}^h \tag{43}$$

$$\boldsymbol{L}_2\boldsymbol{U}^h = \dot{\hat{\boldsymbol{u}}}^h - \hat{\boldsymbol{v}}^h \tag{44}$$

The time-discontinuous Galerkin method has been demonstrated to be unconditionally stable and of third-order accuracy if the $P1$-$P1$ two-field element is used (Hulbert, 1992; 1994; Chien *et al.*, 2000; 2001; 2003).

V. NUMERICAL EXAMPLES

1. Example 1: Axial Transient Analysis of a Rectangular Plate

Consider a 2-D rectangular plate of length 10 m with a width 1 m, as depicted in Fig. 2. The plate is assumed to be fixed at one of its extremities and

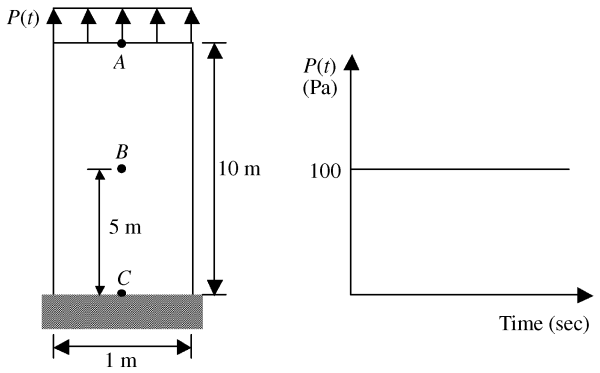

Fig. 2 A rectangular plate subjected to a uniform step transient load (Example 1)

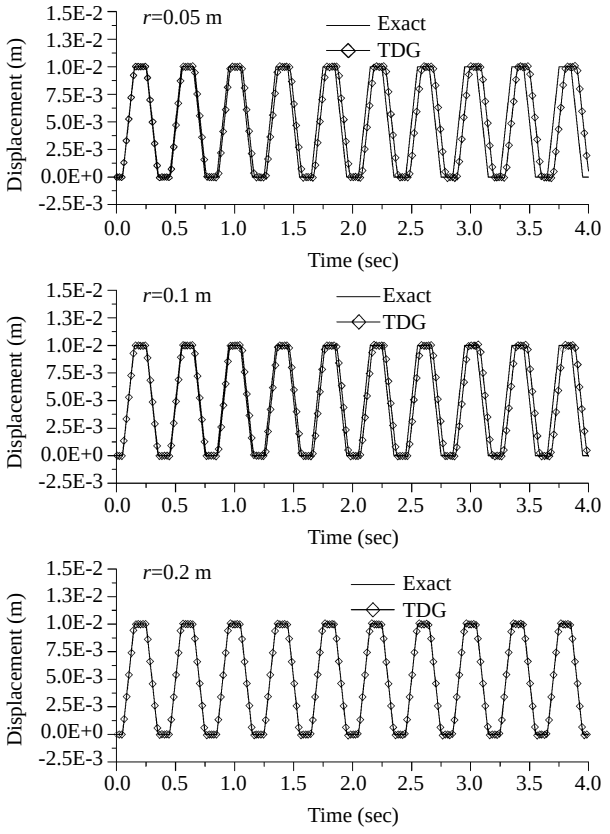

Fig. 3 Displacement responses at point *B* in a rectangular plate corresponding to different sub-domains (Example 1)

subjected to a Heaviside-type tensile load *P* on the other end, as shown in Fig. 2. The material properties used in this problem are Young's modulus E=100 t/m^2, Poisson's ratio ν=0, mass density ρ=10 kg/m^3, and *P*-wave velocity C_p=100 m/sec. In the case of plane stress, the space domain is uniformly discretized by 1111 (11×101) nodes. Each sub-domain is integrated by 8×8 Gauss quadrature. The time step chosen for the integration Δt=0.4/C_p=0.004 sec. The displacement and stress responses in the time history are

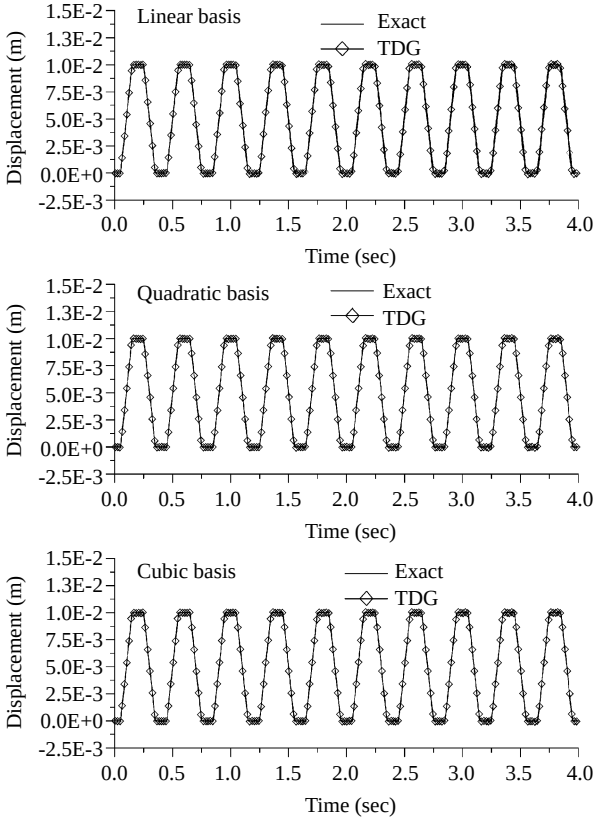

Fig. 4 Displacement responses at point *B* in a rectangular plate using TDG method (Example 1)

analyzed at point *B* in this rectangular plate, as follows.

(i) Effect on the Radii of the Sub-Domains

Figure 3 presents the TDG results for displacement at point *B* with three different radii, 0.05 m, 0.1 m and 0.2 m, and compares them with the exact solution. Note that the TDG solution of the MLPG method accurately approaches the exact solution for the displacement responses, particularly when the time-dependent responses change quickly. Apparently, all the sub-domains with radius r_i=0.05 m or 0.1 m cannot completely contain the solid in the actual problem, and they introduce more period elongation than the TDG solution with a radius of r_i=0.2 m. However, the computational time cost in the analysis by a radius r_i=0.2 m is higher than that with a radius r_i=0.05 m or 0.1 m.

(ii) Effect on the MLS Basis and Integration Method

The sub-domain with radius r_i=0.2m is employed in this analysis to make the whole sub-domains completely cover the solid in the actual problem. Figs. 4 and 6 present for displacement and stress at

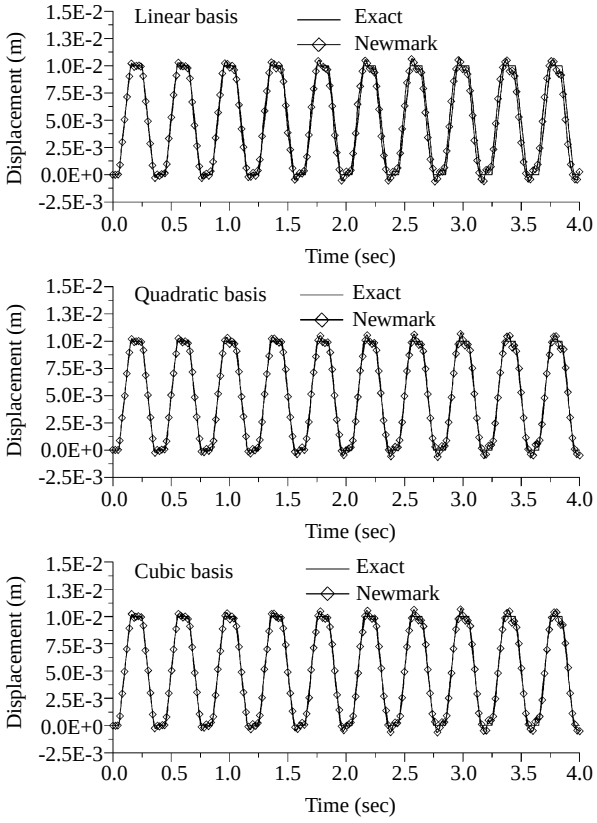

Fig. 5 Displacement responses at point *B* in a rectangular plate using Newmark method (Example 1)

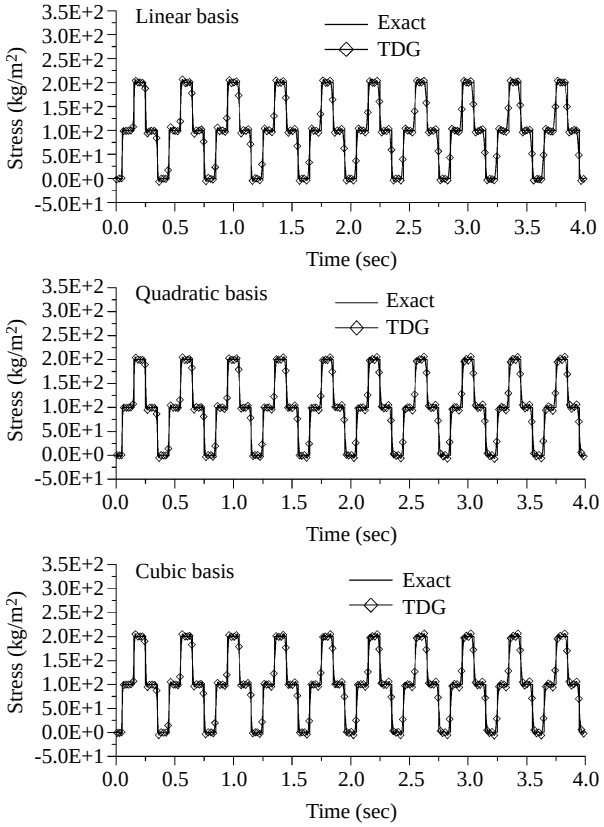

Fig. 6 Stress responses at point *B* in a rectangular plate using TDG method (Example 1)

point *B*, respectively, and compare them with the exact solution corresponding to three different MLS bases (linear, quadratic and cubic). Meanwhile, Figs. 5 and 7 show results of the Newmark method (β= 0.25, γ=0.5; trapezoidal rule) for displacement and stress, respectively, and compare them to the exact solution. Notably, the TDG solution provides the better accuracy of the two methods. The Newmark method cannot control the higher modes and introduces greater period elongation than the TDG method. Additionally, the stress responses obtained using the Newmark method present excessive oscillations, particularly at quick changes of the time-dependent stresses. The advanced bases, such as quadratic or cubic, are employed and the more accurate results are plotted in Figs. 5 and 7, to improve the accuracy of the solutions. The cubic basis for the Newmark method yields the best results among the three bases. However, the TDG method differs a little with three different bases in Figs. 4 and 6. Additionally, the quadratic or cubic basis is twice or three times higher than that of the linear basis in the computational time cost in the analysis by the TDG solution. Even the linear basis used by the TDG method provides very accurate results that the Newmark method cannot achieve.

2. Example 2: Flexural Transient Analysis of a Rectangular Plate

Consider a 2-D solid rectangular plate of length 2 m and a width 2m, as depicted in Fig. 8. The plate is assumed to be fixed at one of its extremities and subjected to an end flexural load of $p(t)$ with a triangular time variation at the other end, as shown in Fig. 8. The numerical values adopted in this problem are t=0.2 sec and p=10 Pa, and the material properties are Young's modulus E=100 t/m^2, Poisson's ratio ν= 0.25, mass density ρ=10 kg/m^3, and P-wave velocity C_p=100 m/sec. In the case of plane stress, the space domain is discretized by 105 nodes on linear and quadratic bases. Each sub-domain is also integrated using 8×8 Gauss quadrature. The closed-form elastodynamic solution to such a problem has not been presented in the literature. Hence, the finite element method (FEM) with 105 nodes (of 80 Q4 elements) or 369 nodes (of 320 Q4 elements) is compared with the MLPG method (Δt=0.02 sec), with linear and quadratic bases. Fig. 9 displays the displacement responses of the time history at point *A* in this rectangular plate. Fig. 9 also shows that the results before time t=2 sec are the same among the four methods. The difference between results after time t=2 sec obtained using the

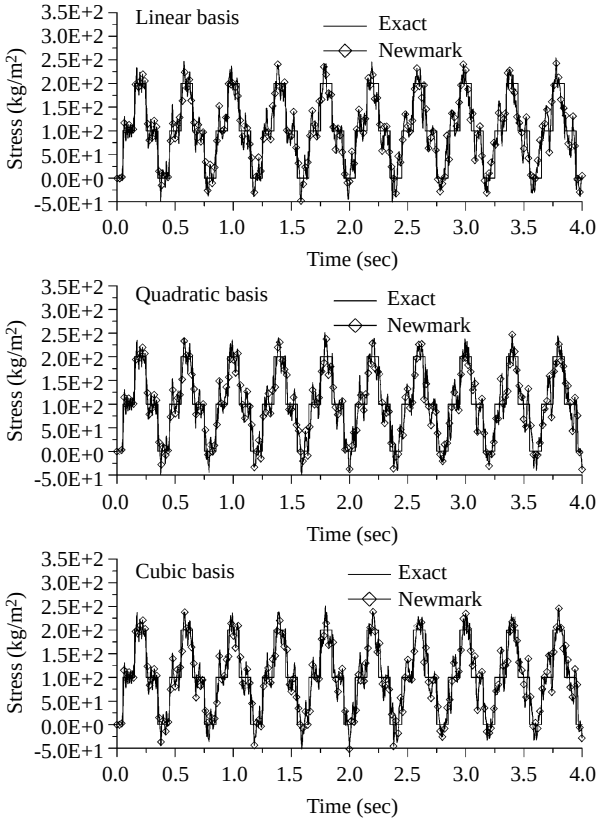

Fig. 7 Stress responses at point *B* in a rectangular plate using Newmark method (Example 1)

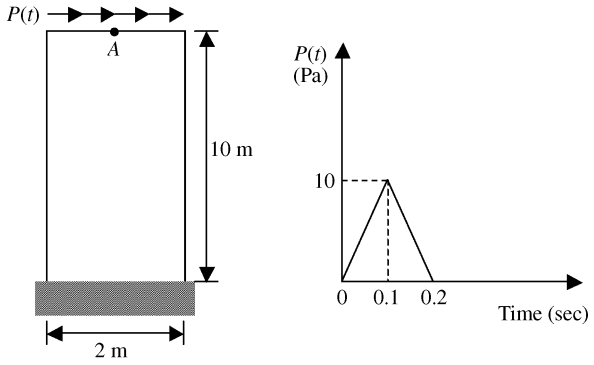

Fig. 8 A rectangular plate subjected to a uniform flexural and triangular pulse load (Example 2)

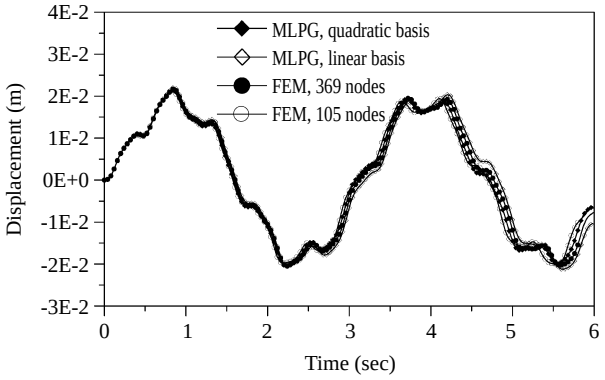

Fig. 9 Displacement responses at point *A* in a rectangular plate (Example 2)

MLPG method with a quadratic basis and those obtained using the FEM with 369 nodes is negligible. However, a great disparity exists between the MLPG method with a linear basis and the FEM with 105 nodes.

VI. CONCLUSIONS

The MLPG method for solving problems in 2-D elastodynamics, based on a local symmetric weak form and the moving least squares approximation, is developed and numerically implemented. This formulation is solved by the time-discontinuous Galerkin method, in which both the unknown displacements and unknown velocities are approximated as piecewise linear interpolation functions in the time domain. The MLPG method is substantially more accurate in determining the displacements and stresses than the finite element method. No element connectivity is needed; and only randomly distributed nodal points are constructed. Moreover, the TDG algorithm using *P*1-*P*1 elements achieves third-order accuracy and exhibits the asymptotic annihilation property. Numerical results further indicate that the solution technique based on time-discontinuous finite element procedure is computationally more stable and more accurate than the solution procedure based on the commonly used algorithms. The proposed method can be extended to the implementation of 3-D elastodynamic problems and boundary node method solution algorithm.

ACKNOWLEDGMENTS

The authors would like to thank the National Science Council of the Republic of China for financially supporting this research under Contract No. NSC 92-2211-E-033-008.

REFERENCES

Atluri, S. N., Kim, H. G., and Cho, J. Y., 1999, "A Critical Assessment of the Truly Meshless Local Petrov-Galerkin (MLPG), and Local Boundary Integral Equation (LBIE) Methods," *Computational Mechanics*, Vol. 24, No. 5, pp. 348-372.

Atluri, S. N., and Zhu, T. L., 1998, "A New Meshless Local Petrov-Galerkin (MLPG) Approach in Computational Mechanics," *Computational Mechanics*, Vol. 22, No. 2, pp. 117-127.

Atluri, S. N., and Zhu, T. L., 2000, "The Meshless Local Petrov-Galerkin (MLPG) Approach for Solving Problems in Elasto-statics," *Computational Mechanics*, Vol. 25, No. 2, pp. 169-179.

Belyschko, T., Lu, Y. Y., and Gu, L., 1994, "Element-Free Galerkin Methods," *International Journal for Numerical Methods in Engineering*, Vol. 37, pp. 229-256.

Belytschko, T., Krongauz, Y., Fleming, M., Organ, D., and Liu, W. K., 1996, "Smoothing and Accelerated Computations in the Element-Free Galerkin Method," *Journal of Computational and Applied Mathematics*, Vol. 74, No. 5, pp. 111-126.

Breitkopf, P., Rassineux, A., Touzot, G., and Villon, P., 2000, "Explicit Form and Efficient Computation of MLS Shape Functions and Their Derivatives," *International Journal for Numerical Methods in Engineering*, Vol. 48, No. 3, pp. 451-466.

Chien, C. C., and Wu, T. Y., 2000, "An Improved Predictor/Multi-Corrector Algorithm for a Time-Discontinuous Galerkin Finite Element Method in Structural Dynamics," *Computational Mechanics*, Vol. 25, No. 5, pp. 430-437.

Chien, C. C., and Wu, T. Y., 2001, "A Particular Integral BEM/Time-Discontinuous Galerkin FEM Methodology for Solving 2-D Elastodynamic Problems," *International Journal of Solids and Structures*, Vol. 38, No. 6, pp. 289-306.

Chien, C. C., Yang, C. S., and Tang, J. H., 2003, "Three-Dimensional Transient Elastodynamic Analysis by a Space and Time-Discontinuous Galerkin Finite Element Method," *Finite Elements in Analysis and Design*, Vol. 39, No. 7, pp. 561-580.

Hulbert, G. M., 1992, "Time Finite Element Methods for Structural Dynamics," *International Journal for Numerical Methods in Engineering*, Vol. 33, pp. 307-331.

Hulbert, G. M., 1994, "A Unified Set of Single-Step Asymptotic Annihilation Algorithms for Structural Dynamics," *Computer Methods in Applied Mechanics and Engineering*, Vol. 113, pp. 1-9.

Lancaster, P., and Salkauskas, K., 1981, "Surfaces Generated by Moving Least Squares Methods," *Mathematics of Computations*, Vol. 37, pp. 141-158.

Liu, W. K., Jun, S., and Zang, Y. F., 1995,"Reproducing Kernel Particle Methods," *International Journal for Numerical Methods in Fluids*, Vol. 20, pp. 1081-1106.

Nayroles, B., Touzot, G., and Villon, P., 1992, "Generalizing the Finite Element Method: Diffuse Approximation and Diffuse Elements," *Computational Mechanics*, Vol. 10, pp. 307-318.

Sladek, J., Sladek, V., and Keer, R. V., 2003, "Meshless Local Boundary Integral Equation Method for 2D Elastodynamic Problems," *International Journal for Numerical Methods in Engineering*, Vol. 57, No. 2, pp. 235-249.

Zhu, T. L., and Atluri, S. N., 1998, "A Modified Collocation Method and a Penalty Formulation for Enforcing the Essential Boundary Conditions in the Element Free Galerkin Method," *Computational Mechanics*, Vol. 21, No. 3, pp. 211-222.

Manuscript Received: Jun. 20, 2003
Revision Received: Nov. 27, 2003
and Accepted: Dec. 03, 2003